Exp Fluids (2015) 56:140
DOI 10.1007/s00348-015-2007-6

RESEARCH ARTICLE

Laser-induced micro-jetting from armored droplets

J. O. Marston[1] · S. T. Thoroddsen[2]

Received: 15 April 2015 / Revised: 31 May 2015 / Accepted: 2 June 2015 / Published online: 23 June 2015

Abstract We present findings from an experimental study of laser-induced cavitation within a liquid drop coated with a granular material, commonly referred to as "armored droplets" or "liquid marbles." The cavitation event follows the formation of plasma after a nanosecond laser pulse. Using ultra-high-speed imaging up to 320,610 fps, we investigate the extremely rapid dynamics following the cavitation, which manifests itself in the form of a plethora of micro-jets emanating simultaneously from the spaces between particles on the surface of the drop. These fine jets break up into droplets with a relatively narrow diameter range, on the order of 10 μm.

1 Introduction

Laser-induced cavitation is a non-intrusive method that can be exploited to produce bubbles inside a liquid or near a liquid free surface following the formation of point plasma in a repeatable manner and has been reported for a variety of experimental investigations; Apitz and Vogel (2005) studied the ejection of material during the ablation of water and other soft materials when a laser pulse was focused near the free surface. In confined geometries, Ando et al. (2012) and Quinto-Su et al. (2009) have investigated the dynamics of bubbles in micro-fluidic channels. One particular feature of cavitation bubbles of interest is the production of jets during the collapse phase, which has been investigated for bubbles induced by both sparks (e.g., Obreschkow et al. 2006; Karri et al. 2012) and laser pulses (Obreschkow et al. 2011).

The generation of high-speed jets and sprays from a liquid free surface via laser-induced cavitation was reported by Thoroddsen et al. (2009) and Heijnen et al. (2009) by focusing a laser pulse into a sessile, hemispherical drop. The initial ejecta sheet, resulting from the plasma near the free surface, emanated at speeds up to 1.4 km/s, whilst fine jets from micro-bubbles sitting under the surface were observed to reach 500 m/s, highlighting the explosive nature of the process. This phenomena was later reproduced in a different experimental setup, using small capillary tubes by Tagawa et al. (2012), where they reported slender jets with speeds up to 850 m/s. Other studies in this area include the explosion of aerosol (free) water droplets by focusing a laser pulse into the droplet (e.g., Kafalas and Herrmann 1973; Armstrong 1984; Chitanvis 1986; Eickmans et al. 1987; Hsieh et al. 1987; Carls and Brock 1988); however, the best representative images of this process are those by Lindinger et al. (2004), where a femtosecond laser pulse was focused into a freely falling water droplet. Some of the first theoretical developments in the area of hydrodynamics resulting from explosive fragmentation include the works of Yarin et al. (Entov et al. 1985, 1986; Sultanov and Yarin 1986, 1988, 1990).

By varying the laser intensity, a range of dynamics was observed from small, single jets to complete atomization. Further to the study by Thoroddsen et al. (2009), Chen et al. (2013) also studied the jet formation resulting from

Electronic supplementary material The online version of this article (doi:10.1007/s00348-015-2007-6) contains supplementary material, which is available to authorized users.

✉ J. O. Marston
jeremy.marston@ttu.edu

[1] Department of Chemical Engineering, Texas Tech University, Lubbock, TX 79409, USA

[2] Division of Physical Sciences and Engineering, King Abdullah University of Science and Technology, Thuwal 23955-6900, Saudi Arabia

a laser pulse focused beneath a flat free surface, showing either slender, stable jets with crown-like formations or rather diffuse, scattered jetting depending on the cavitation bubble depth and maximum bubble radius. Zhiyuan et al. (2014) attempted to characterize the spray following a laser pulse focused into either water or glycerol targets by performing analysis on the spray. In particular, by examining the size of the resulting droplets, they concluded that laser ablation of liquids is highly dependent on viscosity.

In contrast to a laser pulse focused into a pure liquid drop or at a flat free surface, a laser pulse focused into the interior of a particle-laden interface exhibits a qualitatively different result with a plethora of micro-jets produced simultaneously very soon after the pulse. Figure 1 shows an overview of this process for a water droplet coated with hydrophobic glass beads (left panel) and a pure water droplet (right panel). Particle-laden droplets provide a model, highly controllable shell with tunable elastic properties, which stabilize the droplet from coalescence and evaporation (e.g., Zeng et al. 2006; Aussillous and Quere 2006). Irradiation of particle-laden interfaces using UV light is a technique that can be used to trap particles at a surface (e.g., Paunov 2003) for the purpose of determining contact angles. However, irradiation of particle-laden interfaces using intense visible light appears to produce a very dramatic effect. It is this phenomena which we explore herein. Further motivation stems from the process of needle-free injections, which are now evolving to use multiple simultaneous jets as a means of achieving better drug dispersion.

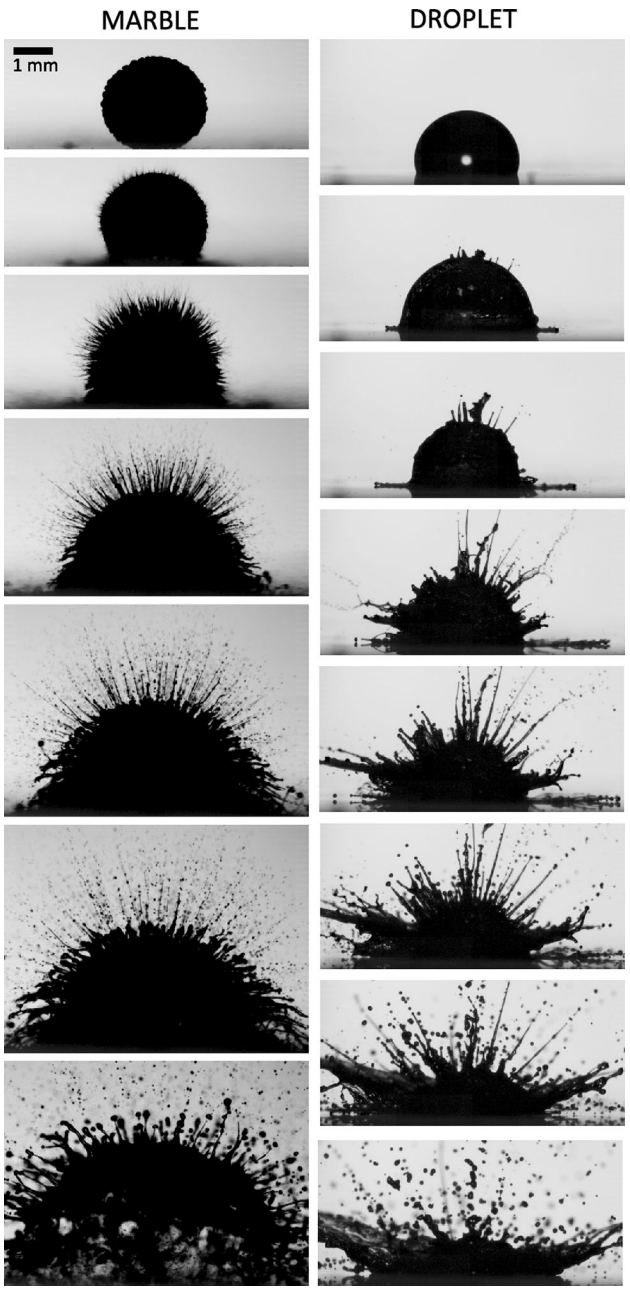

Fig. 1 Image sequences from videos recorded at 101,449 fps for ablation of a liquid marble and 100,000 fps for ablation of a pure water droplet, respectively. The frames shown are taken at times **a** $t = -5, 5, 10, 35, 50, 75, 150\,\mu s$ and **b** $t = -10, 90, 140, 240, 340, 440, 640, 940\,\mu s$ from the laser pulse. The laser beam is focused into the marble/droplet (sitting on a glass substrate) from below with an energy of 38 mJ and focal distance $\delta = 11$ mm. The pulse occurs between the first two images for each sequence. See also the supplemental video 1

2 Experimental

The general experimental setup is shown schematically in Fig. 2a, whilst the two different laser orientations are shown in Fig. 2b, c. A Phantom V1610 (Vision Research) high-speed video camera was used to capture the events, which was triggered externally by the Q-switch output from the laser. The laser (Big Sky Laser Ultra 50) has a wavelength of 532 nm and a pulse duration of 7 ns. The initial beam diameter is 3 mm and is focused through a 10× objective lens. The pulse energy, E_p, is controlled by manually setting the Q-switch delay which, at 143 µs, renders a maximum energy of 38 mJ per pulse, measured by an optical power meter (Melles Griot). Herein, we study a range of output energies down to 1 mJ per pulse. In all cases, the event was initiated manually using a remote interface to fire a single pulse. Calibration images indicate that the focus spot size is approximately 300 µm in diameter, yielding a radiant exposure of 54 J/cm^2 at maximum power.

A Leica Z16 APO long-working-distance microscope with variable magnification was fitted with a long-pass filter to block the laser light, whilst background illumination was achieved using a single metal halide light source guided through a fiber optic bundle onto a diffuser screen behind the marbles, thus rendering high-contrast silhouette images.

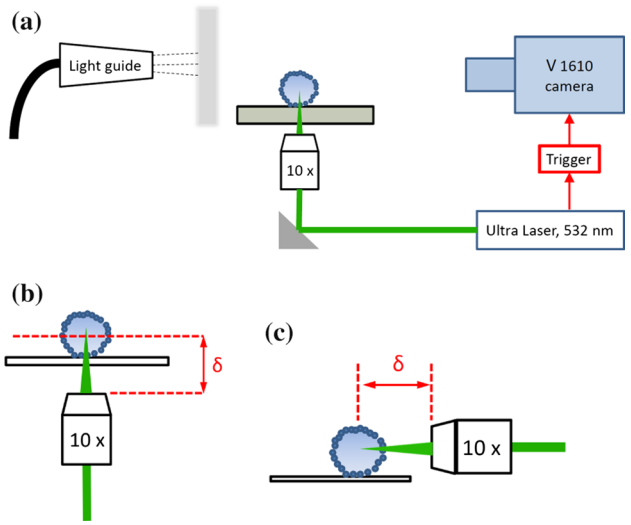

Fig. 2 **a** Schematic representation of the experimental setup. **b** Laser pulse from below and **c** laser pulse from the side. In both (**b**) and (**c**), δ is the distance from the objective lens to the centerline of the marble

Armored droplets (a.k.a liquid marbles) were prepared by allowing a liquid droplet (volume of 10 µl, radius of 1.3 mm) to impact on a small bed of hydrophobic glass beads (mean diameter $d_g = 149\,\mu\text{m}$, $d_{10} = 125\,\mu\text{m}$, $d_{90} = 176\,\mu\text{m}$, mean circularity 0.92) after which the drop was manually rolled along the bed surface to ensure a complete encapsulation. The marble was then gently deposited on the surface of a microscope slide above a 10× objective lens, through which the laser beam was focused. Figure 3a shows an image of the surface of a liquid marble in contact with the glass microscope slide. Image analysis of multiple such images indicated that the surface packing fraction was approximately 79 % for our experiments. Furthermore, side-view images of isolated particles residing at the interface, such as that shown in Fig. 3b, indicate that the contact angle measured by the protrusion length, $l = r(1 - \cos\theta)$, is $\theta = 120°$. However, as highlighted by the arrows, there is an upward-facing meniscus, which thus renders a concave interfacial shape to the liquid between particles (discussed in more detail later).

The moment the laser pulse hits the marble can be identified from the video due to the extremely bright emission of light caused by the generation of plasma (Thoroddsen et al. 2009), as shown in Fig. 4. This moment is taken as the reference time, $t = 0$.

Following the interesting results of Thoroddsen et al. (2009) and Tagawa et al. (2012) for the jet-speed dependence on the location of the focal spot of the laser relative to the free surface, we performed a subset of experiments, whereby the distance from the objective lens to the centerline of the marble was varied. We use this measure of distance, as shown in Fig. 2b, c, since we cannot accurately determine the laser focal spot location in this experimental configuration.

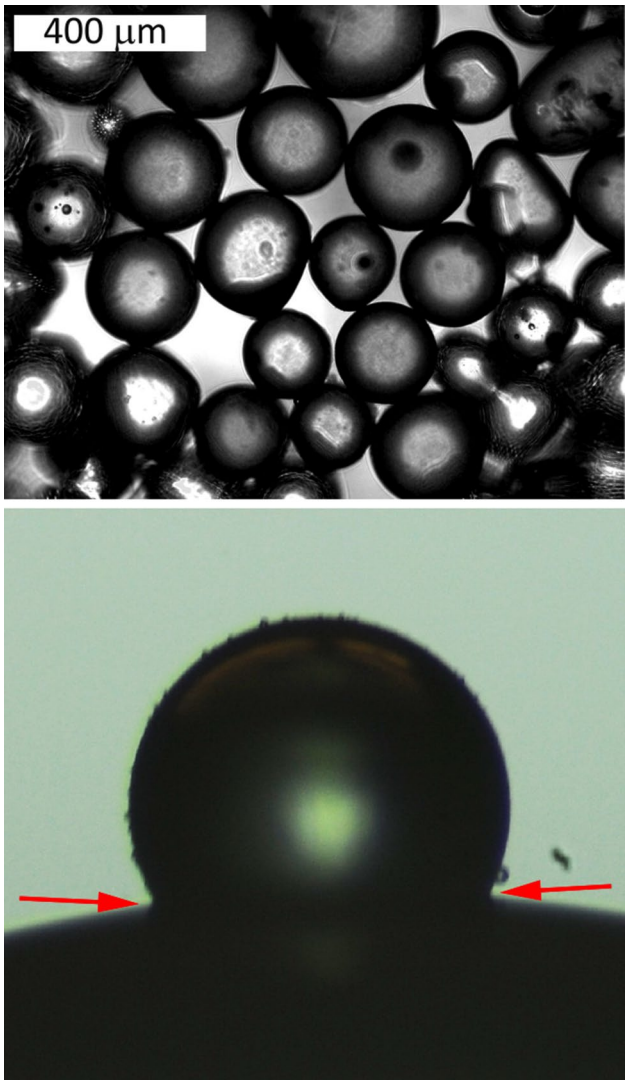

Fig. 3 *Top* microscope image of the surface of a liquid marble formed from a water droplet coated with hydrophobic glass beads with mean size $d_g = 149\,\mu\text{m}$. *Bottom* image of an isolated particle on the drop surface for measuring protrusion and contact angle; the *red arrows* highlight the upward-facing meniscus

3 Qualitative observations

3.1 Laser pulse from below

To highlight the dramatic influence of the particle shell, Fig. 1b shows the ablation of a pure water droplet without a shell of particles. In this instance, the droplet volume, laser energy and focal distance are the same as in Fig. 1a for the armored droplet.

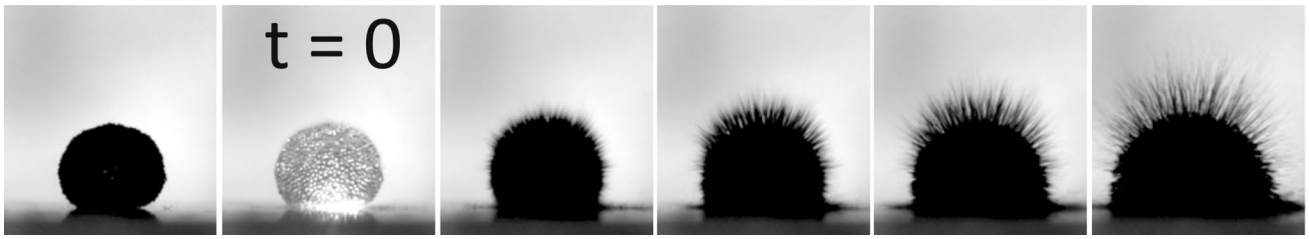

Fig. 4 Example image sequence showing an internally illuminated marble, indicating that the laser pulse ($E_p = 38$ mJ, $\delta = 11$ mm, from below) hits within this video frame. The time between frames is 9.85 μs

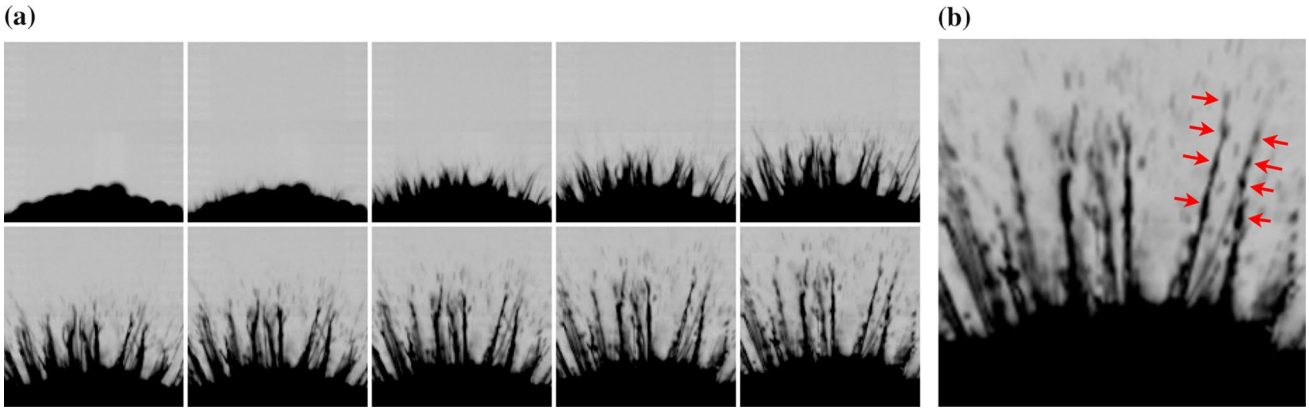

Fig. 5 **a** Image sequence from a video recorded at 320,610 fps. The time between frames 1 and 2 is 6.2 and 3.1 μs thereafter. The jets emerge at speeds up to 50 m/s. **b** Final image from the sequence shown in (**a**), with *arrows* indicating the formation of satellite drops as the jet breaks up. $E_p = 38$ mJ, $\delta = 11$ mm

We note the distinct lack of high-speed jets during the first 100 μs, seen for the armored droplets, but the ejection of several jets *after* the collapse of the cavitation bubble shown at $t = 210$ μs. This phenomena was also reported by Thoroddsen et al. (2009), where the collapse of the cavitation bubble also occurred around 200 μs after the laser pulse. These jets emerge at speeds ranging from 25 to 62 m/s. Thus, even though the speeds are comparable to those observed for the armored droplets, the qualitative differences lie in the timescales *and* the fact that there are only several such high-speed jets, whereas for the armored droplets, the high-speed jetting is uniform across the entire surface. This is further illustrated in Fig. 5 which shows images from an ultra-high-speed video recorded at 320 kfps for the early evolution of the jets from armored droplets. The jets shown are largely still intact for the duration of this sequence but show signs of becoming unstable toward the end of the sequence, approximately 30 μs after the laser pulse as highlighted by the red arrows in Fig. 5b.

Following the breakup of the jets, a plethora of microscopic satellite droplets are observed, which travel away from the droplet. These satellite droplets have a fairly narrow size range, typically with radii between 7 and 50 μm, with most between 5 and 20 μm, as shown in Fig. 6. This size range is larger than those seen in the spray emitted by pure droplet ablation (typical sizes 2.5–4.5 μm) due to the fact that droplets herein emanate from the discrete jets, rather than the cylindrical ejecta sheet in the case of the ablation of pure droplets (e.g., Thoroddsen et al. 2009). The speeds of these droplets are measured by particle tracking techniques in Sect. 4.

Once into the regime of micro-jetting, i.e., $E_p > E_P^*$ and $\delta < \delta^*$ (discussed in Sect. 3.3), where the $*$ indicates the threshold above/below which micro-jetting is observed, we also observed a high-speed spray emerging from the base of the marble, which travels along the surface of the microscope slide at speeds up to 100 m/s over the first few frames, as shown in Fig. 7. The origins of this spray are clarified by experiments, wherein the laser pulse strikes from the side, as per Sect. 3.2.

3.2 Laser pulse from the side

Figure 8 shows a typical sequence from a high-speed video recorded at 100,000 fps where the laser pulse is focused into the marble from the side, as per the schematic in Fig. 2c.

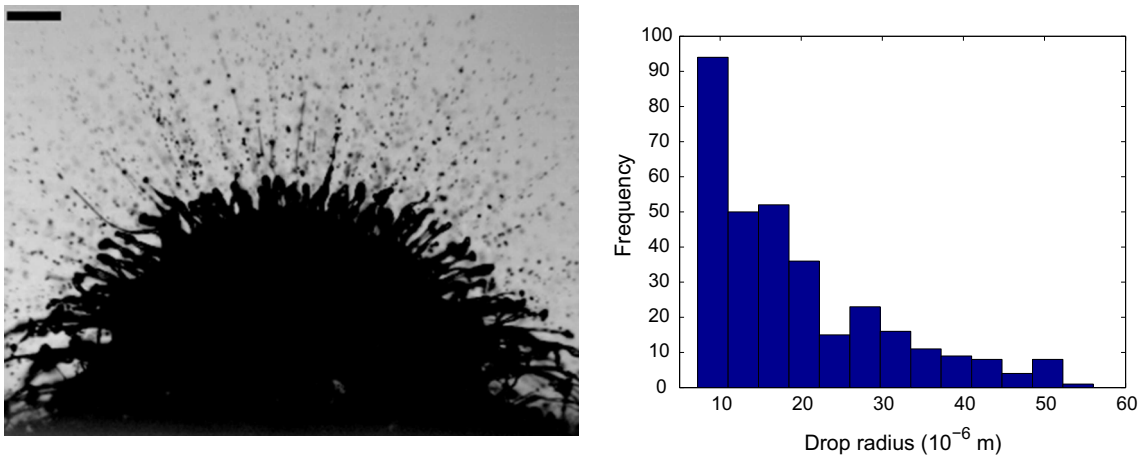

Fig. 6 **a** Image taken at $t = 88\,\mu$s showing a range of drop sizes produced after the breakup of the micro-jets. The *scale bar* is 500 μm. Drop radii are between 7 and 50 μm. $E_p = 38$ mJ, $\delta = 11$ mm

Fig. 7 Frames showing the high-speed spray emerging along the surface of the microscope slide following a laser pulse from below. The *scale bar* is 1 mm. $t = 0, 10, 20$ and 30 μs. $E_p = 38$ mJ, $\delta = 11$ mm

Interestingly, in this realization, we observe that only the right-hand side of the marble surface is compromised, i.e., no micro-jetting is seen, whilst the remainder of the marble is left in tact for duration of this sequence (50 μs). Clearly, we still observe the rapid ejection of some small satellite droplets, e.g., in frames 4 and 5 in the right column; however, the spray is directed toward the laser. This explains the origins of the high-speed spray seen in Fig. 7, which emerges horizontally for a laser pulse from below—the spray directed toward the laser pulse is forced to move horizontally along the microscope slide. From the sequence in Fig. 8, we estimate that the spray emerges at speeds over 300 m/s. The absence of the micro-jetting from the left-hand side of the marble (i.e., opposite to where the laser pulse strikes) indicates that the plasma spot and subsequent cavitation are localized to the right-hand side in this case with $\delta = 16$ mm. Note also that particles are also ejected from the surface along with liquid jets and droplets for this configuration (also seen in Fig. 10b).

3.3 Critical energy and focal distance

Given the lack of micro-jetting observed from the opposite side of the armored droplet in Fig. 8, we performed a series of experiments for both configurations (laser from below and from the side) to investigate the critical conditions for micro-jetting. Figure 9a shows images taken 50 μs after the laser pulse for a range of values of δ, the distance between the objective lens and the marble equator as per Fig. 2b, for laser pulses from below. Noting that the working distance of this focusing lens is 16 mm, $\delta = 16$ mm means that the focal spot should be precisely in the center of the marble. However, we observe that this does not result in the explosive jet formation as for smaller values of δ. In fact, there appears to be a transition around $\delta \approx 13$ mm, where we observe some droplet ejection but no fast jets; then, for $\delta \leq 11$ mm, we observe the rapid micro-jetting phenomena as in Figs. 1, 4 and 5.

This critical value of δ is confirmed by a similar variation in δ for by changing the laser orientation to the side, shown in Fig. 9b. Again, we observe no jetting for $\delta > 16$ mm, but the ejection of some small droplets for $\delta = 13$ mm. However, the high-speed micro-jetting only occurs once $\delta < 11.5$ mm. This is consistent with the observations shown in Fig. 9a for various values of δ. The physical basis for this critical focal distance is presumed to be due to a confluence of the focal point of the laser beam within the marble being closer the surface nearest to the marble and the blocking of a significant portion of

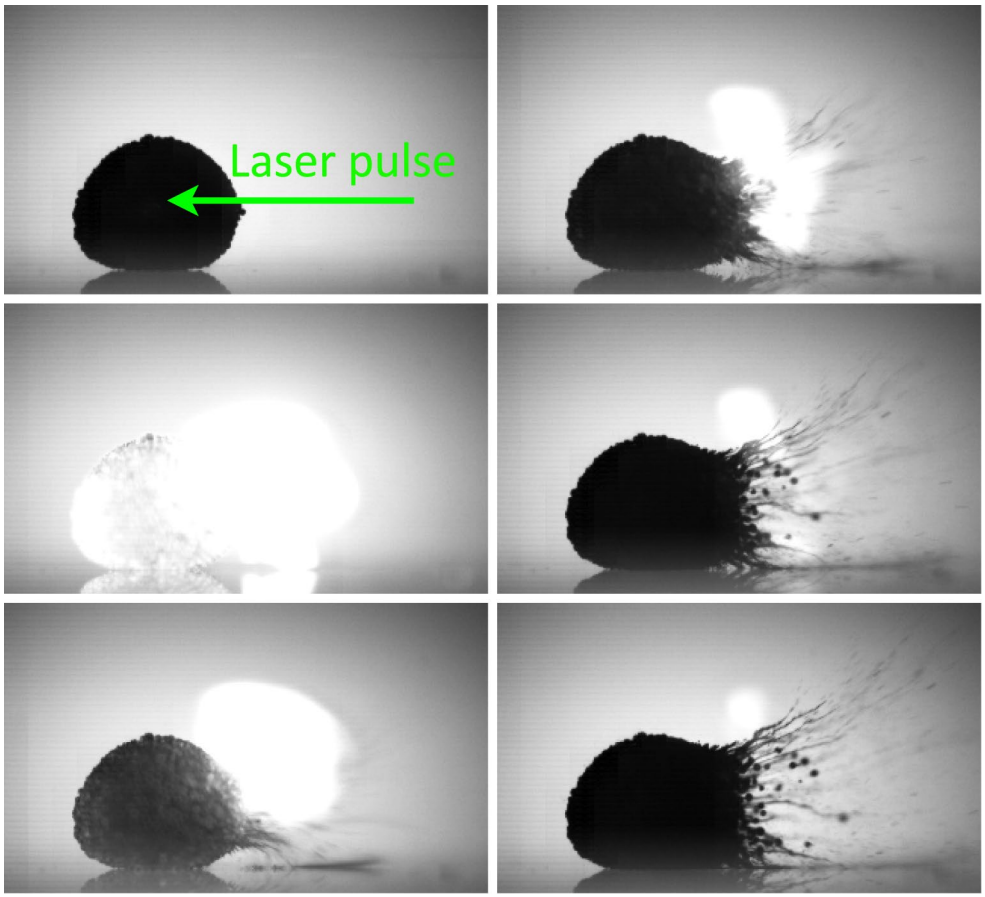

Fig. 8 Image sequence showing the result of a laser pulse focused into a marble from the side with $\delta = WD = 16$ mm. The pulse comes from the *right* and is focused at the spot indicated by the end of the *green arrow* in the first image. The marble is 3 mm in diameter, and all images are 10 μs apart. The *bright white area* in frames 2–6 is an artifact of the imaging due to the intense emission from the plasma

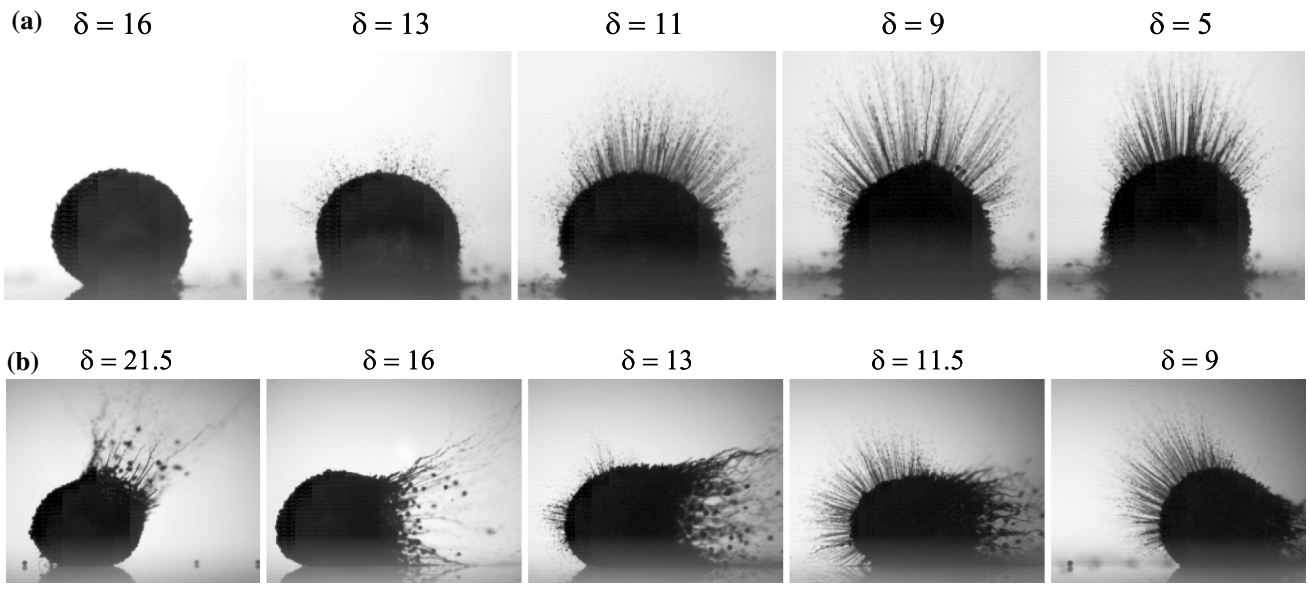

Fig. 9 Images taken 50 μs after the laser pulse ($E_p = 38$ mJ) for a range of distances, δ, indicated in mm above each image. In (**a**) the laser pulse is directed from below, whilst in (**b**) it is from the side

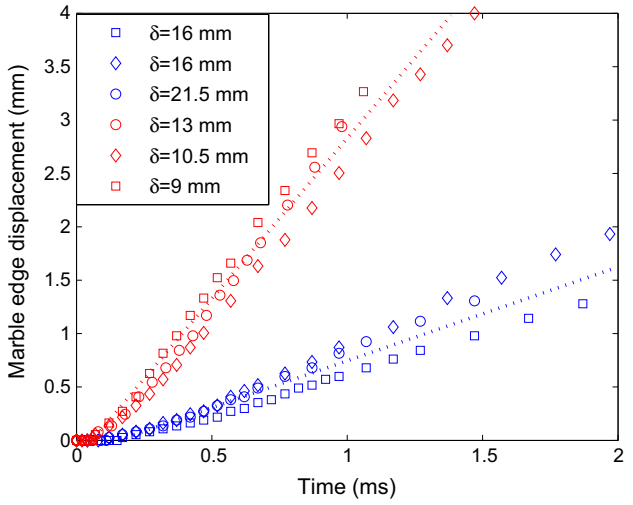

Fig. 10 Forward displacement of marble edge after laser pulse from the side. Various values of δ are shown, all for the maximum laser energy, $E_p = 38$ mJ. The *dotted lines* are to guide the eye only

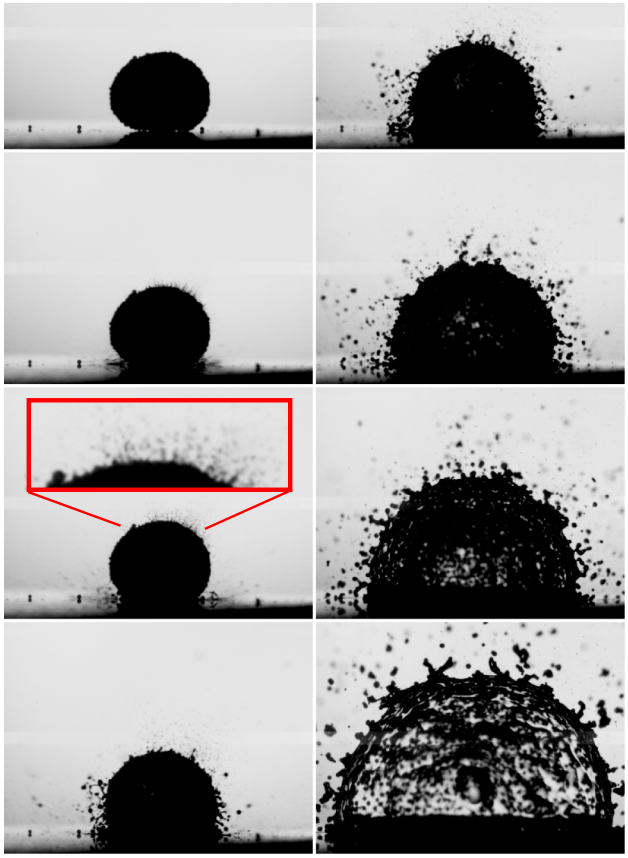

Fig. 11 Select frames from a high-speed video sequence following a laser pulse from below with $E_p = 20.4$ mJ and $\delta = 11$ mm. $t = -20, 20, 40, 120, 160, 280, 480$ and $980\,\mu$s

the focused laser beam by the particles residing at the surface. This reasoning holds for both experimental configurations since the laser beam must always pass through a layer of glass beads regardless of orientation. This conjecture is also supported by examining the post-jetting motion of the droplet as a whole; here, we tracked the opposite edge of the marble (relative to the entrance of the laser pulse). The results, as shown in Fig. 10, indicate a significantly greater velocity, ≈ 2.8 m/s , for trials with $\delta < \delta^*$ compared to ≈ 0.75 m/s for trials with $\delta > \delta^*$, indicating a higher rate of energy conversion from the laser pulse to kinetic energy, i.e., $E_P \rightarrow KE$.

The micro-jetting is also suppressed by decreasing the laser pulse energy, as shown in Fig. 11 for $E_p = 20$ mJ. This sequence demonstrates the absence of the high-speed micro-jets, despite the ultimate ablation of the droplet as a whole. We do observe some droplets ejected from the top of the armored droplet, shown by the zoomed inset image in frame 3 of this sequence, but these typically emerge with low speed. Thus, it is clear that the fast micro-jetting phenomenon is dependent on both focal distance of the spot *and* laser pulse energy. For these experiments, we thus determine the thresholds to be $E_p^* \approx 20.4$ mJ and $\delta^* \approx 11$ mm.

4 Jet and satellite drop speeds

Across the entire parameter space studied, we find that the initial spray, which occurs within the first $50\,\mu$s from the laser pulse, is ejected at speeds from 50 to ~ 300 m/s. The micro-jets typically break up at $t \approx 50$–$100\,\mu$s into a plethora of satellite droplets, as seen in Figs. 1 and 6, after which we can measure their speed using velocimetry techniques. An example of this type of analysis is presented in Fig. 12, showing both raw images and derived velocity fields with speeds up to 36.4 m/s at $t = 70\,\mu$s, where the speeds are first measurable. By compiling data for multiple trials and laser pulse energies, we can plot both the mean satellite drop speeds and range, as shown in Fig. 13. Here, we find a rapid deceleration from $V_{\text{sat}} \approx 30 \rightarrow 10$ m/s as $t = 100 \rightarrow 400\,\mu$s. We note that for satellite drops with diameters $d_{\text{sat}} \approx 10\,\mu$m traveling at $V_{\text{sat}} \approx 30$ m/s, following Marston et al. (2012), we can estimate the deceleration due to air drag as

$$a_{\text{drag}} \approx \frac{3\rho_{\text{air}} V_{\text{sat}}^2}{4 d_{\text{sat}} \rho_{\text{sat}}},$$

indicating that the satellites should decelerate rapidly, with effective decelerations on the order of 1000 g, in accordance with our experimental observations. Using the smallest measured satellite drop diameter of $7\,\mu$m, an initial velocity of 30 m/s at $t = 100\,\mu$s and the above estimate of the

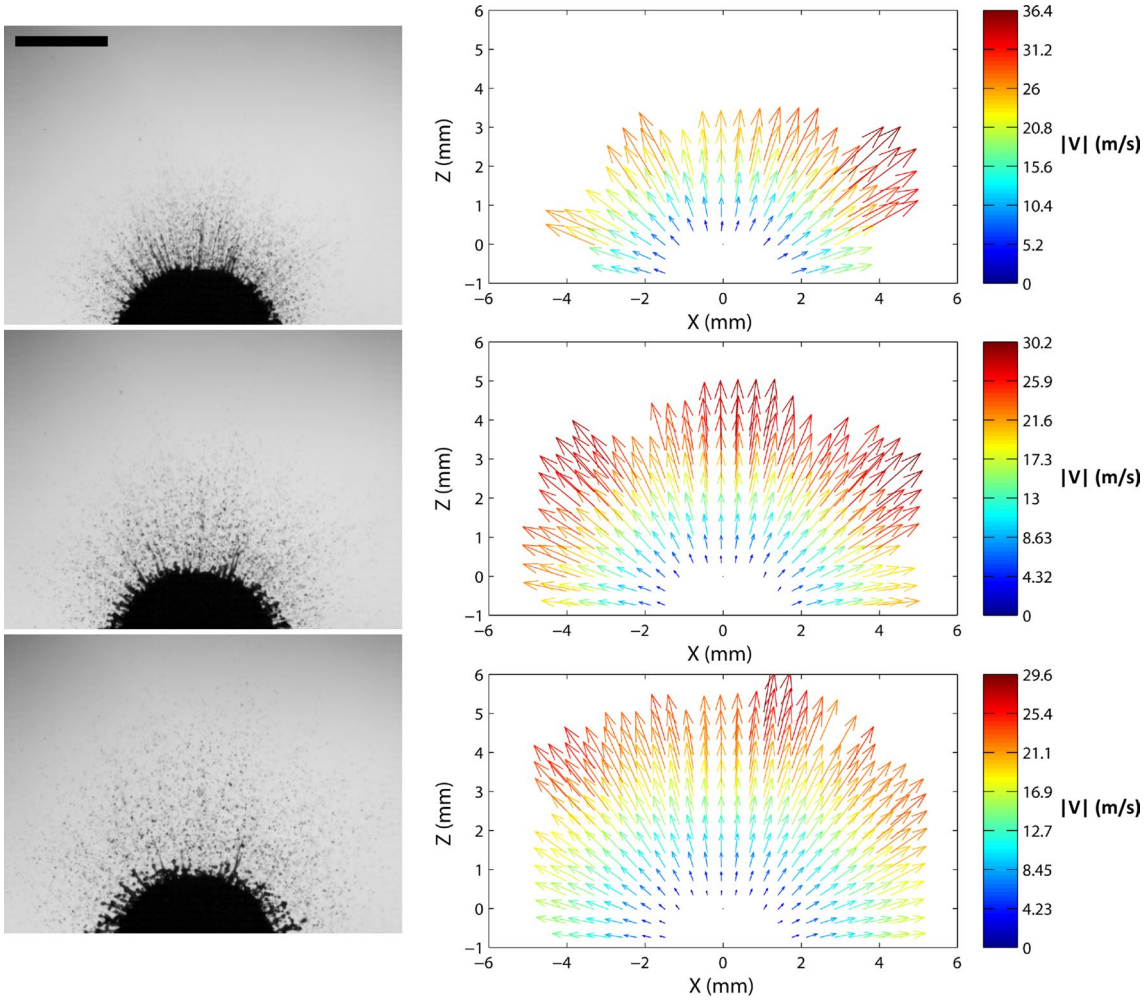

Fig. 12 Raw images and derived velocity fields of satellite droplets ejected after the laser pulse. Taken at times $t = 70, 100$ and $140\,\mu$s after the laser pulse hits the marble. The origin $(x, z) = (0, 0)$ corresponds to the approximate location of the laser focal spot based on visual inspection of the raw video. The *scale bar* is 2 mm long

air drag, a velocity of 13.5 m/s at $t = 400\,\mu$s is predicted, which is close to the measured velocity $V_{\text{sat}} \approx 10$ m/s in Fig. 13.

As with our observations in Fig. 9, once into the regime of micro-jetting, further increasing the laser pulse energy or decreasing the focal distance did not result in any significant variation in satellite drop speed, falling within the ranges shown by the error bars in Fig. 13.

5 Discussion and concluding remarks

We have conducted an experimental study of the cavitation-induced jetting phenomenon when a laser pulse strikes a liquid marble. By varying the pulse energy and distance from the objective lens to the marble, we deduce that the fast micro-jetting described herein occurs for $E_p > 20.4$ mJ and $\delta < 11$ mm. In contrast, once these thresholds are reached, further increasing the pulse energy did not result in any quantifiable effect on jet or drop speeds.

The initial pressure pulse induced by the rapid cavitation event expels high-speed jets from between particles located at the drop surface, whilst at later times, the entire free surface undergoes expansion due to the growth of the bubble inside. Through inspection of the packing structure of the particles at the surface of the drop, we postulate that the jet dynamics is affected by the geometrical packing of the grains, which may influence breakup.

Given that the micro-jets emanating from the armored droplets break up after approximately $30\,\mu$s, we can conclude that their rapid emergence aids stability since the capillary breakup timescale, $\tau \approx 2.91\sqrt{\rho R^3/\sigma}$, where R is the jet radius which is approximately $3\,\mu$s for jets with the observed diameters. This is supported by noting that the jet Weber number, giving the ratio of inertia to surface tension, is of $O(100)$. The Reynolds number of the jets observed

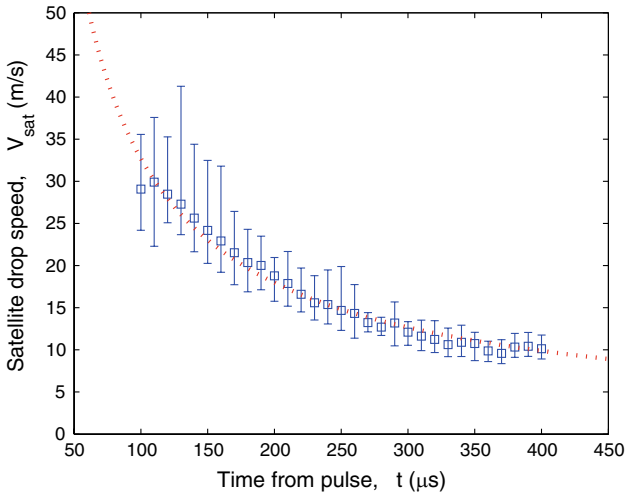

Fig. 13 Mean satellite drop speeds versus time from pulse. The data points correspond to the mean, whilst the *error bars* encompass the full range observed over multiple trials and laser pulse energies. The *dashed red line* indicates the best fit power law with an index of −0.86

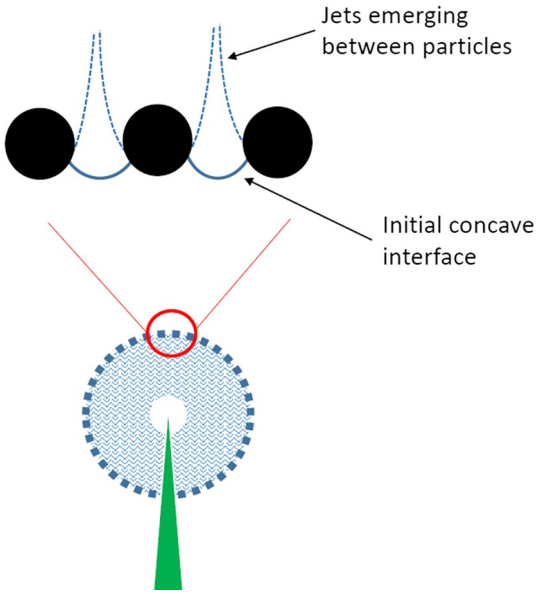

Fig. 14 Schematic of micro-jet formation for armored droplets due to locally concave interfaces between particles

herein is also of $O(100)$, further highlighting the inertial dominance during the early stages of the jetting [see also the smooth micro-jets in Thoroddsen et al. (2009)].

Preliminary tests with powders with smaller mean sizes $d_g \approx 30\,\mu$m indicate that the jetting phenomena reported herein is limited to interfaces with a monolayer of grains at the surface. For powder with grain sizes finer than approximately 100 μm, the cohesive properties make it difficult to produce liquid marbles with just a monolayer. Previous studies (Aussillous and Quere 2006; Gao and McCarthy 2007; Bormashenko et al. 2009; Arbatan and Shen 2011) have shown that water droplets coated with fine silica grains yield approximately the same surface tension as pure water ($\sigma \approx 72$ mN/m).

We note that the Laplace pressure inside the drop is given by $P = P_{\text{atm}} + \frac{2\sigma}{R_0}$, so that rupturing the interface of the marble requires an overpressure of $\Delta P = 2\sigma/R_0$. Based simply on bubble sizes induced by the laser pulse in pure liquid drops, we estimate that the overpressure inside the drop exceeds 1/3 atmospheric pressure, which is easily enough to overcome the confining pressure of $2\sigma/R_0$. This is likely to be a vast underestimate of the true overpressure caused by vapor bubbles (Allen et al. 1985; Deng et al. 2003). The fact that this overpressure occurs so rapidly [typical timescale is O(10)] μs) explains the explosive nature of these experiments.

The difference between droplets coated with particles and those without is quite dramatic, whereby the particle-coated droplets exhibit a much more uniform plethora of micro-jets, which is absent in the case of pure droplets, during the initial expansion of the plasma-driven bubble. The principle reason for this is due to the local structure of the interface between particles, as shown in Fig. 14. The concave nature of the interfaces between the particles, similar to the internal vapor bubbles in Thoroddsen et al. (2009) and the experiments in capillary tubes by Tagawa et al. (2012), is responsible for the focusing of energy into liquid jets [see also Antkowiak et al. 2007].

Due to particles residing at the interface, we could not directly observe the interior dynamics immediately following the laser pulse; however, given that the jets emerge so rapidly (within 10 μs) and before the bulk of the marble begins to move, it seems reasonable that the micro-jets are a product of the shock wave interaction with the concave interfaces located between the particles on the surface, as shown in Fig. 14, as proposed by both Thoroddsen et al. (2009) and Tagawa et al. (2012).

Further experiments in more well-defined geometries and planar particle-laden interfaces for the purpose of aerosol formation are the subject of continuing work.

References

Allen RR, Meyer JD, Knight WR (1985) Thermodynamics and hydrodynamics of thermal ink jets. Hewlett-Packard 36:21–27

Ando K, Liu A-Q, Ohl C-D (2012) Homogenous nucleation in water in microfluidic channels. Phys Rev Lett 109:044501

Antkowiak A, Bremond N, Le Dizes S, Villermaux E (2007) Short-term dynamics of a density interface following an impact. J Fluid Mech 577:241–250

Apitz I, Vogel A (2005) Material ejection in nanosecond Er:YAG laser ablation of water, liver, and skin. Appl Phys A 81:329–338

Arbatan T, Shen W (2011) Measurement of the surface tension of liquid marbles. Langmuir 27:12923–12929

Armstrong RL (1984) Aerosol heating and vaporization by pulsed light beams. Appl Opt 23:148–155

Aussillous P, Quere D (2006) Properties of liquid marbles. Proc R Soc A 462:973–999

Bormashenko E, Pogreb R, Whyman G, Musin A, Bormashenko Y (2009) Shape, vibrations, and effective surface tensions of water marbles. Langmuir 25:1893–1896

Carls JC, Brock JR (1988) Propagation of laser breakdown and detonation waves in transparent droplets. Opt Lett 13:273–275

Chen RCC, Yu YT, Su KW, Chen JF, Chen YF (2013) Exploration of water jet generated by Q-switched laser induced water breakdown with different depths beneath a flat free surface. Opt Express 21:445–453

Chitanvis SM (1986) Explosion of water droplets. Appl Opt 25:1837–1839

Deng P, Lee Y-K, Cheng P (2003) The growth and collapse of a micro-bubble under pulse heating. Int J Heat Mass Transf 46:4041–4050

Eickmans JH, Hsieh W-F, Chang RK (1987) Laser-induced explosion of H_2O droplets: spatially resolved spectra. Opt Lett 12:22–24

Entov VM, Sultanov FM, Yarin AL (1985) Breakup of liquid films under the action of a pressure drop in the ambient gas. Sov Phys Dokl 30:882

Entov VM, Sultanov FM, Yarin AL (1986) Disintegration of liquid films subjected to an ambient gas pressure difference. Fluid Dyn 21(3):376–383

Gao L, McCarthy TJ (2007) Ionic liquid marbles. Langmuir 23:10445–10447

Heijnen L, Quinto-Su PA, Zhao X, Ohl C-D (2009) Cavitation within a droplet. Phys Fluids 21:091102

Hsieh W-F, Zheng J-B, Wood CF, Chu BT, Chang RK (1987) Propagation velocity of laser-induced plasma inside and outside a transparent droplet. Opt Lett 12:576–578

Kafalas P, Herrmann J (1973) Dynamics and energetics of the explosive vaporization of fog droplets by a 10.6-μm laser pulse. Appl Opt 12:772–775

Karri B, Ohl S-W, Klaseboer E, Ohl C-D, Khoo BC (2012) Jets and sprays arising from a spark-induced oscillating bubble near a plate with a hole. Phys Rev E 86:036309

Lindinger A, Hagen J, Socaciu LD, Bernhardt TM, Woste L, Duft D, Leisner T (2004) Time-resolved explosion dynamics of H_2O droplets induced by femtosecond laser pulses. Appl Opt 43:5263

Marston JO, Li E-Q, Thoroddsen ST (2012) Evolution of fluid-like granular ejectas generated by sphere impact. J Fluid Mech 704:5–36

Obreschkow D, Kobel P, Dorsaz N, de Bosset A, Nicollier C, Farhat M (2006) Cavitation bubble dynamics inside liquid drops in microgravity. Phys Rev Lett 97:094502

Obreschkow D, Tinguely M, Dorsaz N, Kobel P, de Bosset A, Farhat M (2011) Universal scaling law for jets of collapsing bubbles. Phys Rev Lett 107:204501

Paunov VN (2003) Novel method for determining the three-phase contact angle of colloid particles adsorbed at air–water and oil–water interfaces. Langmuir 19:7970–7976

Quinto-Su P, Lim KY, Ohl C-D (2009) Cavitation bubble dynamics in microfluidic gaps of variable height. Phys Rev E 80:047301

Sultanov FM, Yarin AL (1986) Radial expansion of cylindrical layers of viscous and rheologically complex fluids. J Eng Phys Thermophys 50(6):645–652

Sultanov FM, Yarin AL (1988) Rayleigh–Taylor instability of expanded polymer films. J Appl Mech Tech Phys 29(3):409–414

Sultanov FM, Yarin AL (1990) Droplet size distribution in a percolation model for explosive liquid dispersal. J Appl Mech Tech Phys 31(5):708–713

Tagawa Y, Oudalov N, Visser CW, Peters IR, van der Meer D, Sun C, Prosperetti A, Lohse D (2012) Highly focused supersonic microjets. Phys Rev X 2:031002

Thoroddsen ST, Takehara K, Etoh TG, Ohl C-D (2009) Spray and microjets produced by focusing a laser pulse into a hemispherical drop. Phys Fluids 21:112101

Zeng C, Bissig H, Dinsmore AD (2006) Particles on droplets: from fundamental physics to novel materials. Solid State Commun 139:547–556

Zhiyuan Z, Hua G, Zhenjun F, Jie X (2014) Characteristics of droplets ejected from liquid propellants ablated by laser pulses in laser plasma propulsion. Plasma Sci Technol 16:251–254